

# Measurement of the $K^+ \rightarrow \pi^0 \mu^+ \nu_\mu \gamma$ Branching Ratio

S. Adler,<sup>1</sup> A.O. Bazarko,<sup>2,\*</sup> P.C. Bergbusch,<sup>3</sup> E.W. Blackmore,<sup>4</sup> D.A. Bryman,<sup>3</sup> S. Chen,<sup>4,†</sup> I-H. Chiang,<sup>1</sup> M.V. Diwan,<sup>1</sup> J.S. Frank,<sup>1</sup> T. Fujiwara,<sup>5,‡</sup> J.S. Haggerty,<sup>1</sup> J. Hu,<sup>4</sup> T. Inagaki,<sup>6</sup> M.M. Ito,<sup>2,§</sup> D.E. Jaffe,<sup>1</sup> V. Jain,<sup>1,¶</sup> S. Kabe,<sup>6</sup> S.H. Kettell,<sup>1</sup> P. Kitching,<sup>7</sup> M. Kobayashi,<sup>6</sup> T.K. Komatsubara,<sup>6</sup> A. Konaka,<sup>4</sup> Y. Kuno,<sup>6,\*\*</sup> M. Kuriki,<sup>6,††</sup> K.K. Li,<sup>1</sup> L.S. Littenberg,<sup>1</sup> J.A. Macdonald,<sup>4,‡‡</sup> P.D. Meyers,<sup>2</sup> J. Mildenerger,<sup>4</sup> M. Miyajima,<sup>8</sup> N. Muramatsu,<sup>9</sup> T. Nakano,<sup>9</sup> C. Ng,<sup>1,§§</sup> S. Ng,<sup>7</sup> T. Nomura,<sup>5,¶¶</sup> T. Numao,<sup>4</sup> J.-M. Poutissou,<sup>4</sup> R. Poutissou,<sup>4</sup> G. Redlinger,<sup>4,\*\*\*</sup> T. Sato,<sup>6</sup> K. Shimada,<sup>8</sup> T. Shimoyama,<sup>8</sup> T. Shinkawa,<sup>6,†††</sup> F.C. Shoemaker,<sup>2,‡‡</sup> J.R. Stone,<sup>2</sup> R.C. Strand,<sup>1</sup> S. Sugimoto,<sup>6</sup> Y. Tamagawa,<sup>8</sup> T. Tsunemi,<sup>6,‡‡‡</sup> C. Witzig,<sup>1</sup> and Y. Yoshimura<sup>6</sup>

(E787 Collaboration)

<sup>1</sup>Brookhaven National Laboratory, Upton, New York 11973

<sup>2</sup>Joseph Henry Laboratories, Princeton University, Princeton, New Jersey 08544

<sup>3</sup>Department of Physics and Astronomy, University of British Columbia, Vancouver, British Columbia, Canada, V6T 1Z1

<sup>4</sup>TRIUMF, 4004 Wesbrook Mall, Vancouver, British Columbia, Canada, V6T 2A3

<sup>5</sup>Department of Physics, Kyoto University, Kitashirakawa, Sakyo, Kyoto 606-8502, Japan

<sup>6</sup>High Energy Accelerator Research Organization (KEK), Oho, Tsukuba, Ibaraki 305-0801, Japan

<sup>7</sup>Centre for Subatomic Research, University of Alberta, Edmonton, Canada, T6G 2N5

<sup>8</sup>Department of Applied Physics, Fukui University, 3-9-1 Bunkyo, Fukui, Fukui 910-8507, Japan

<sup>9</sup>Research Center for Nuclear Physics, Osaka University, 10-1 Mihogaoka, Ibaraki, Osaka 567-0047, Japan

(Dated: April 9, 2010)

A measurement of the decay  $K^+ \rightarrow \pi^0 \mu^+ \nu_\mu \gamma$  has been performed with the E787 detector at Brookhaven National Laboratory. Forty events were observed in the signal region with the background expectation of  $(16.5 \pm 2.7)$  events. The branching ratio was measured to be  $(1.58 \pm 0.46(stat.) \pm 0.08(syst.)) \times 10^{-5}$  in the kinematic region  $E_\gamma > 30$  MeV and  $\theta_{\mu\gamma} > 20^\circ$ , where  $E_\gamma$  is the energy of the emitted photon and  $\theta_{\mu\gamma}$  is the angle between the muon and the photon in the  $K^+$  rest frame. The results were consistent with theoretical predictions.

PACS numbers: 13.20.Eb, 12.39.Fe

## I. INTRODUCTION

A measurement of the decay  $K^+ \rightarrow \pi^0 \mu^+ \nu_\mu \gamma$  ( $K_{\mu 3\gamma}$ ) has been performed using the E787 apparatus [1] at the Alternating Gradient Synchrotron (AGS) of Brookhaven National Laboratory. This decay is due to radiative ef-

fects in the semi-leptonic transition of  $K^+ \rightarrow \pi^0 \mu^+ \nu_\mu$  decay ( $K_{\mu 3}$ ). The decay  $K_{\mu 3\gamma}$  can proceed via inner bremsstrahlung (IB) in which a photon is emitted from the charged particle in the initial or final state, and structure-dependent radiative decay (SD) which involves the emission of a photon from the intermediate states in the hadronic transition from  $K^+$  to  $\pi^0$ . For hadron decays in the energy region below 1 GeV, the effective-field approach based on chiral symmetry, chiral perturbation theory (ChPT) [2], is applicable [3]. At  $O(p^4)$  in ChPT, a partial branching ratio  $BR(K_{\mu 3\gamma}, E_\gamma > 30$  MeV and  $\theta_{\mu\gamma} > 20^\circ)$ , where  $E_\gamma$  is the energy of the emitted photon and  $\theta_{\mu\gamma}$  is the angle between the muon and the photon in the  $K^+$  rest frame, is predicted to be  $2.0 \times 10^{-5}$  [4, 5]. The relative size of SD contribution is around 8 %.

The first search for  $K_{\mu 3\gamma}$ , which was performed in 1973 [6] with  $K^+$  decays at rest in a heavy-liquid bubble chamber, obtained  $BR(K_{\mu 3\gamma}, E_\gamma > 30$  MeV)  $< 6.1 \times 10^{-5}$  at the 90% confidence level (C.L.). The  $K^- \rightarrow \pi^0 \mu^- \nu_\mu \gamma$  decay in flight was studied by the ISTR+ spectrometer; the ratio  $BR(K_{\mu 3\gamma})/BR(K_{\mu 3})$  for the region  $30 < E_\gamma < 60$  MeV was found to be  $(4.48 \pm 0.68(stat.) \pm 0.99(syst.)) \times 10^{-4}$  [7]. Based on this value, the Particle Data Group cited  $BR(K_{\mu 3\gamma}, 30 < E_\gamma < 60$  MeV) as  $(1.5 \pm 0.4) \times 10^{-5}$  [8]. The  $K^+ \rightarrow \pi^0 \mu^+ \nu_\mu \gamma$  decay at rest was studied with the toroidal spectrometer of the E246 and E470 experiments at the KEK 12-GeV proton synchrotron; the

\*Present address: Schlumberger, Princeton Jct., NJ 08550.

†Present address: Department of Engineering Physics, Tsinghua University, Beijing 100084, China.

‡Electronic address: fujiwara@scphys.kyoto-u.ac.jp

§Present address: Thomas Jefferson National Accelerator Facility, Newport News, VA 23606.

¶Present address: Department of Physics, Indiana University, Bloomington, IN 47405-7105.

\*\*Present address: Department of Physics, Osaka University, Toyonaka, Osaka 560-0043, Japan.

††Present address: Graduate School of Advanced Sciences of Matter, Hiroshima University, Hiroshima 739-8530, Japan.

‡‡Deceased

§§Also at Physics Department, State University of New York at Stony Brook, Stony Brook, NY 11794-3800.

¶¶Present address: High Energy Accelerator Research Organization (KEK).

\*\*\*Present address: Brookhaven National Laboratory.

†††Present address: Department of Applied Physics, National Defense Academy, Yokosuka, Kanagawa 239-8686, Japan.

‡‡‡Present address: Department of Physics, Kyoto University.

$BR(K_{\mu 3\gamma}, E_\gamma > 30 \text{ MeV and } \theta_{\mu\gamma} > 20^\circ)$  was found to be  $(2.4 \pm 0.5(\text{stat.}) \pm 0.6(\text{syst.})) \times 10^{-5}$  [9].

In this paper, we present results from the E787 experiment at the AGS. We describe the analysis we have performed to observe the  $K^+ \rightarrow \pi^0 \mu^+ \nu_\mu \gamma$  decay and the measurement of the partial branching ratio  $BR(K_{\mu 3\gamma}, E_\gamma > 30 \text{ MeV and } \theta_{\mu\gamma} > 20^\circ)$ . We compare our results to the predictions of ChPT at  $O(p^4)$ . The  $BR(K_{\mu 3\gamma}, 30 < E_\gamma < 60 \text{ MeV})$  was also determined and can be compared with the previous result. The spectra of  $K_{\mu 3\gamma}$  observables based on ChPT at  $O(p^4)$  [4, 5] are shown in Fig. 1 and are consistent with the spectra given in [10].

## II. DETECTOR

E787 was a rare kaon-decay experiment studying  $K^+ \rightarrow \pi^+ \nu \bar{\nu}$  [11–13] and related decays [14, 15] using  $K^+$  decays at rest. The data for the  $K_{\mu 3\gamma}$  measurement were acquired during the 1998 run [13] of the AGS, using kaons of 710 MeV/c incident on the E787 apparatus at a rate of about 4 MHz. Two stages of electrostatic particle separation in the beam line [16] reduced the pion contamination at the E787 apparatus to 25%. The incident kaons were detected and identified by a Čerenkov counter, multi-wire proportional chambers and a beam counter. After being slowed by a BeO degrader, 27% of the kaons came to rest in an active stopping target located at the center of the detector system [17] in a 1.0 Tesla solenoidal magnet (Fig. 2).

The 12-cm diameter target, which consisted of 0.5-cm square plastic scintillating fibers, provided initial tracking of the stopping kaon as well as the charged decay products. They passed through a 0.64-cm thick layer of plastic scintillation counters surrounding the target (I-counters). A  $3 \times 10^{-2}$  radiation length ( $X_0$ ) thick cylindrical drift-chamber [18] provided tracking information for momentum determination. The charged particles lost energy in an array of plastic scintillation counters called the Range Stack (RS), which provided a measurement of kinetic energy and range (equivalent cm of plastic scintillator) of the charged track. The RS was segmented into 24 azimuthal sectors and 21 radial layers, totaling one  $X_0$ . The RS counters in the first layer (T-counters), which were 0.635-cm thick and 52-cm long, defined the solid angle acceptance for the charged track in the RS. The subsequent RS counters in the second layer (L2-counters) and beyond were 1.905-cm thick and 182-cm long. The RS counter in the sector and layer where the track came to rest was called the “stopping counter”. The RS counters were read out by phototubes attached to the upstream and downstream ends; the output pulse shapes were recorded by 500-MHz sampling transient digitizers (TDs) [19], which provided precise time and energy information for the hits in each counter.

Photons from kaon decays at rest in the target were detected by a hermetic calorimeter system surrounding

the central region. The cylindrical barrel (BL) calorimeter, which was located immediately outside the RS and covered two thirds of the solid angle, was used to reconstruct and measure the three photons from the  $K_{\mu 3\gamma}$  decay (i.e. two photons from the  $\pi^0$  and the radiative photon). The BL calorimeter consisted of alternating layers of lead (0.1-cm thick) and plastic scintillator (0.5-cm thick) sheets, and about 29% of the electromagnetic shower energy was deposited in the scintillators. The BL was segmented azimuthally into 48 sectors and, in each sector, four radial groups of 16, 18, 20 and 21 lead-scintillator layers, respectively with increasing radius, formed BL modules totaling 14.3  $X_0$ . The modules were 190-cm in length along the beam axis. They were read out by phototubes attached to the upstream and downstream ends, and the outputs were recorded by time-to-digital converters (TDCs) and analogue-to-digital converters (ADCs). The two endcap calorimeters [20], additional “collar” calorimeters for filling minor openings along the beam direction, and any active parts of the detector not hit by the charged track were used for detecting extra particles.

## III. TRIGGER

The signature of the  $K_{\mu 3\gamma}$  decay was a kaon decay at rest with a charged track in the RS and three electromagnetic showers in the BL calorimeter. The kinetic energy of most of the muons from  $K_{\mu 3\gamma}$  after requiring  $E_\gamma > 30 \text{ MeV}$  and  $\theta_{\mu\gamma} > 20^\circ$  (Fig. 1) is less than 85 MeV; thus, we used the RS counters in the first six layers for the muon measurement. The RS counters in the 7th layer and beyond were used to detect extra particles or reject photons whose showers started before reaching the BL.

In the trigger for the  $K_{\mu 3\gamma}$  decay, the “3 $\gamma$  trigger”, a kaon was identified by a coincidence of hits from the Čerenkov counter, beam counter and target. To guarantee that the kaon actually decayed at rest, the timing of the outgoing particle (via the I-counters) was required to be at least 1.5 nsec later than the timing of the incoming kaon (via the Čerenkov counter). A positively charged track was required to have a coincidence of the hits from the I-counters, a T-counter and an L2-counter in the same RS sector (T-2 sector), and from the counters in the 3rd or 4th RS layer in the T-2 sector or in either of the next two clockwise sectors. The tracks reaching the 7th or 8th layer were rejected. With such trigger conditions, only tracks for which the RS stopping counter was located in the 3rd to the 6th layer, corresponding to the muons with momentum 100-160 MeV/c, were accepted.

In order to count the number of showers in the BL calorimeter online, the analog sum of the outputs from 8 modules in two adjacent sectors, separately for the upstream and downstream ends, were accepted with a threshold corresponding to about 5 MeV of visible energy per end. The discriminator outputs were OR-ed for either end, and then fed into a logic unit. The number

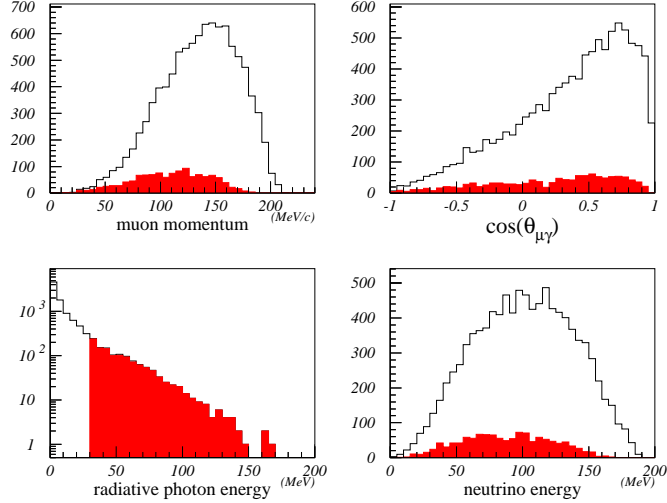


FIG. 1: Spectra of  $K^+ \rightarrow \pi^0 \mu^+ \nu_\mu \gamma$  observables based on ChPT at  $O(p^4)$ : muon momentum (top left), cosine of  $\theta_{\mu\gamma}$  (top right),  $E_\gamma$  (bottom left) and neutrino energy (bottom right). The unhatched and hatched histograms represent the distributions before and after imposing the conditions  $E_\gamma > 30$  MeV and  $\theta_{\mu\gamma} > 20^\circ$ .

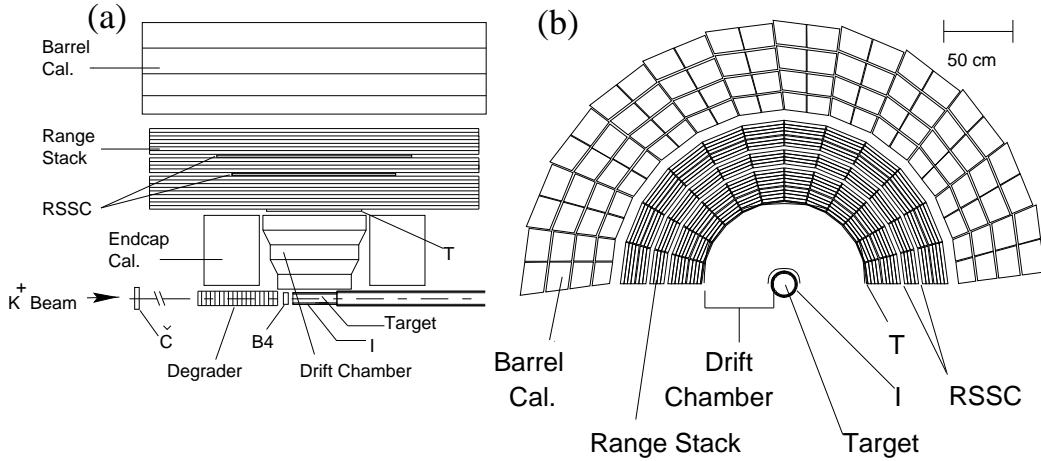


FIG. 2: Schematic side(a) and end(b) views showing the upper half of the E787 detector. Č: Čerenkov counter; B4: beam counter; I and T; trigger scintillation counters (I-counters and T-counters). Range-stack straw-tube tracking chambers (RSSC) were unused in this measurement.

of showers was required to be equal to three or larger. An event was rejected online if the visible energy in the endcap calorimeters was more than 20 MeV, the energy in the RS sectors outside the region of the charged track was more than 10 MeV, or the energy in the RS counters from the 9th to 21st layers in any sector was larger than the level for minimum ionizing particles.

The  $3\gamma$  trigger was prescaled by five for taking data simultaneously with the trigger for  $K^+ \rightarrow \pi^+ \nu \bar{\nu}$ . Approximately 6 events per slow-extracted beam (2.2-sec duration) from the AGS in every 4.2 sec were recorded. A total exposure of kaons entering the target available for the  $K_{\mu 3\gamma}$  measurement was  $3.5 \times 10^{11}$ . A total of

$9.4 \times 10^6$  triggered events were collected.

Monte Carlo simulation was performed to generate samples of  $K_{\mu 3\gamma}$  as well as other kaon decays at rest in the E787 detector system. The simulation package developed for E787 was comprised of the electromagnetic-shower simulation routines from EGS4 [21], the routines to model other physics processes such as particle decays and charged-particle interactions in the detector elements, and the routines to simulate the trigger conditions. The events in the Monte Carlo samples can be analyzed with the same analysis codes for real data, except that the information on the pulse shapes in the digitizers and the information on the outputs from most of the

beam instrumentation were not stored. The Monte Carlo simulation of E787 is described in [22].

## IV. EVENT RECONSTRUCTION

### A. Basic reconstruction

The charged track was reconstructed and measured with a standard algorithm used in the  $K^+ \rightarrow \pi^+ \nu \bar{\nu}$  analysis of E787 described in [22], except that the charged particle was assumed to be a muon and all the energy deposited in the RS stopping counter was attributed to the muon track coming to rest<sup>1</sup>. The initial momentum was determined by correcting the momentum measured in the drift chamber for the energy loss suffered by the muon based on the observed track length in the target. The kinetic energy was determined by adding up the energy deposits of the muon track in the scintillators of the target and the RS, taking account of the energy loss in inactive materials such as wrapping and chamber materials. The range was calculated from the track length in the target and in the RS, and was used for muon identification in the  $K_{\mu 3\gamma}$  analysis. Events were discarded if the momentum of the charged particle was larger than 190 MeV/c. Many of the triggered events were due to the  $K^+ \rightarrow \pi^+ \pi^0$  decay for which the  $\pi^+$  had interactions within the RS counters before coming to rest; these events were easily rejected because the  $\pi^+$  momentum (205 MeV/c) was measured with the drift chamber.

The isolated showers in the BL calorimeter were reconstructed and the timing, energy and direction of the photons were measured with the same algorithm used in the analysis of E787 and E949 (the successor experiment to E787) [22–26] for kaon decays with photons in the final states [14, 15, 24]. The muon track in the RS defined the event time reference, and adjacent BL modules whose timing was within  $\pm 6$  nsec of the track time and whose visible energy was more than 0.2 MeV were grouped into a “cluster”. In each module, the energy was measured as the geometrical mean of the visible energies divided by the calibrated visible fraction (0.292) in the upstream and downstream ends. The hit position in the end view of the detector was determined by the segmentation of the modules; the hit position along the beam axis ( $z$ ) was measured from the end-to-end time and energy differences. The location of the shower in the BL was obtained by taking an energy-weighted average of the hit positions in the same cluster and, in conjunction with the kaon decay vertex position in the target, the azimuthal angle and the polar angle with respect to the

beam axis were determined for each photon. In the  $K_{\mu 3\gamma}$  analysis, if two showers were separated by less than 55 cm and the energy of one of them was less than 25 MeV, they were combined to a single shower in order to avoid misidentifying a part of an electromagnetic shower to be a separate one. Events were discarded unless three or four showers were observed in the BL calorimeter.

### B. Primary selection

Selection criteria (“cuts”) were imposed to make sure that the trigger conditions were satisfied and the kaon in the initial state and the muon and photons in the final state were reconstructed within the fiducial volume of the detector system. Furthermore, cuts on the timing and energy of the hits recorded in the Čerenkov counter, proportional chambers, beam counter and the target, including an offline delayed-coincidence cut which required  $> 2$  nsec between the muon time and the kaon time measured in the target, were imposed to remove the events triggered by kaon decays in flight or by multiple beam particles into the detector. From the triggered events,  $1.1 \times 10^6$  events survived and were used in the subsequent analysis.

## V. BACKGROUND SOURCES

Kaon decays with a single charged track in the region 100–160 MeV/c and at least one  $\pi^0$  in the final state, i.e.,  $K_{\mu 3}$ ,  $K^+ \rightarrow \pi^+ \pi^0 \gamma$  ( $K_{\pi 2\gamma}$ ),  $K^+ \rightarrow \pi^0 e^+ \nu_e$  ( $K_{e3}$ ),  $K^+ \rightarrow \pi^0 e^+ \nu_e \gamma$  ( $K_{e3\gamma}$ ) and  $K^+ \rightarrow \pi^+ \pi^0 \pi^0$  ( $K_{\pi 3}$ ), are potential background sources. They are classified as follows:

- “ $K_{\mu 3-1}$ ”:  $K_{\mu 3}$  decays associated with an extra cluster in the BL due to accidental hits.
- “ $K_{\mu 3-2}$ ”:  $K_{\mu 3}$  decays associated with an extra cluster in the BL when the showers due to the two photons from  $\pi^0$  were reconstructed as three showers.
- “ $K_{\pi 2\gamma}$ ”:  $K_{\pi 2\gamma}$  decay events in which the  $\pi^+$  was misidentified as a muon or decayed in flight before it came to rest in the RS.
- “ $K_{e3(\gamma)}$ ”:  $K_{e3\gamma}$  decays for which the  $e^+$  was misidentified as a muon, or  $K_{e3}$  decays with the  $e^+$  misidentification and an extra cluster in the BL or a photon due to bremsstrahlung.
- “ $K_{\pi 3}$ ”:  $K_{\pi 3}$  decays in which the  $\pi^+$  was misidentified as a muon or decayed in flight before it came to rest in the RS, and at the same time one of the four photons from two  $\pi^0$ 's was undetected.

Background due to multiple beam particles scattering into the detector simultaneously was found to be negligible.

<sup>1</sup> In the  $\pi^+$  track reconstruction, the presence of the additional 4 MeV deposit in the RS stopping counter due to the  $\pi^+ \rightarrow \mu^+ \nu$  decay at rest was assumed and was subtracted from the observed energy.

In the subsequent two sections, the cuts to improve the signal-to-background and measure the background are described. The cuts were developed with the sample of real data prescaled by three and the Monte Carlo samples. The studies of these samples confirmed that the expected number of candidate events in the signal region was larger than the background expectation. The cuts were then imposed to the entire dataset.

## VI. EVENT SELECTION

### A. Selection of the muon and three photons

For muon identification, a cut based on the measured range compared to that expected given the measured muon momentum was imposed. The measured range was also compared to the measured kinetic energy. Furthermore, to reject  $e^+$  tracks in the RS, a set of cuts that checked the consistency between the measured energy and range in each of the RS counters, the  $dE/dx$  cuts, were employed.

For the  $K_{\mu 3\gamma}$  decay, events were discarded unless exactly three showers with  $> 5$  MeV were observed in the BL calorimeter within  $\pm 2$  nsec of the muon track time in the RS. The photon energy should also be sufficiently larger than the online energy threshold; since the threshold had been applied to the analog-sum signals separately for the upstream and downstream ends (Section III), the threshold level depended on the  $z$  position of the shower in the BL. Thus the photon energy was required to be greater than 23 (66) MeV for the showers located at the edge (center) of the BL.

In order to remove the events with the photon due to bremsstrahlung of the  $e^+$  track from the  $K_{e3}$  or  $K_{e3\gamma}$  decay within the RS, we calculated the angle between the direction of the hit position of the charged track at the RS T-counter from the center of the detector system and the direction of each of the photons from the kaon decay vertex position. The minimum of the angles should be larger than  $26^\circ$  (“ $e^+$  bremsstrahlung” cut).

An extra photon could disappear through inefficiency due to very narrow gaps between counters or inactive material. Tight photon-detection requirements, the “photon veto” cuts, were imposed on the detector subsystems; hits in coincidence with the track time within a few nsec and with the energy above a threshold of typically 1 MeV were identified as the activity due to an extra photon. The photon veto cuts also ensured that only those events in which the total photon energy from the  $K_{\mu 3\gamma}$  decay was deposited in the BL (and a part of the showers was not recorded in any other subsystem) were accepted.

An extra photon could also go undetected when two electromagnetic showers in the BL overlapped each other and were reconstructed as a single cluster (“fused cluster”). In the Monte Carlo studies of  $K_{\pi 3}$ , it was confirmed that the case with the overlap of two photons originated from the same  $\pi^0$  was negligible; thus the

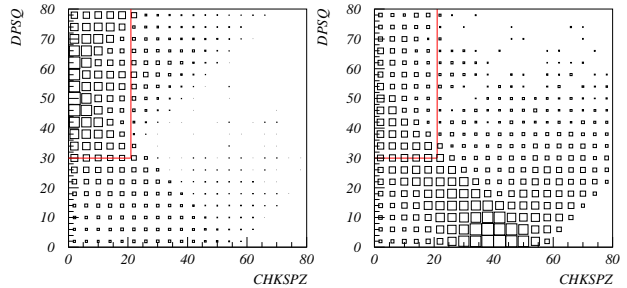


FIG. 3: Plots of the variables  $DPSQ$  vs.  $CHKSPZ$  for the  $K_{\mu 3\gamma}$  events (left) and the  $K_{\pi 3}$  background events (right) generated by the Monte Carlo simulation.

other case, with the overlap of two photons from different  $\pi^0$ 's (“odd combination”), should be considered. We designed two variables  $DPSQ$  and  $CHKSPZ$ , described below, in which the fused cluster from  $K_{\pi 3}$  was characterized. Suppose that one of the three reconstructed photons  $\gamma_1, \gamma_2$  and  $\gamma_3$ , e.g.  $\gamma_1$ , was the fused cluster and consisted of two photons  $\gamma_A$  and  $\gamma_B$  with the same azimuthal and polar angles and with the energies  $E_{\gamma_A} = \epsilon$  and  $E_{\gamma_B} = E_{\gamma_1} - \epsilon$ , where  $\epsilon$  was a parameter that varied from 0 to  $E_{\gamma_1}$ . A pair of invariant masses  $m_{\gamma_A\gamma_2}$  and  $m_{\gamma_B\gamma_3}$  and  $F_1 \equiv \sqrt{(m_{\gamma_A\gamma_2} - m_{\pi^0})^2 + (m_{\gamma_B\gamma_3} - m_{\pi^0})^2}$ , where  $m_{\pi^0}$  is the nominal mass of  $\pi^0$ , were calculated as a function of  $\epsilon$ .  $F_1$  should be small when  $\epsilon$  agreed with the correct value. In the same way,  $F_2$  and  $F_3$  were calculated supposing that  $\gamma_2$  and  $\gamma_3$  were the fused cluster, respectively. Finally, the minimum of  $F_1, F_2$  and  $F_3$  with all the possible values of  $\epsilon$  in each hypothesis, called  $DPSQ$  in this analysis, was obtained.  $DPSQ$  would be small if an event was from  $K_{\pi 3}$  and one of  $\gamma_1, \gamma_2$  and  $\gamma_3$  was the fused cluster. On the other hand, the invariant masses of two out of the three reconstructed photons:  $m_{\gamma_1\gamma_2}, m_{\gamma_2\gamma_3}$  and  $m_{\gamma_3\gamma_1}$  were calculated, and the minimum of  $|m_{\gamma_1\gamma_2} - m_{\pi^0}|, |m_{\gamma_2\gamma_3} - m_{\pi^0}|$  and  $|m_{\gamma_3\gamma_1} - m_{\pi^0}|$ , called  $CHKSPZ$  in this analysis, was obtained. If an event was from  $K_{\pi 3}$  with odd combination, the invariant mass of other two photons should not be close to  $m_{\pi^0}$  and thereby  $CHKSPZ$  would be large. Figure 3 shows the  $DPSQ$  vs.  $CHKSPZ$  plots for the  $K_{\mu 3\gamma}$  events and the  $K_{\pi 3}$  background events (after imposing the BL cuts and the photon veto cuts) generated by the Monte Carlo simulation. To suppress the background,  $DPSQ$  was required to be more than 30 MeV/ $c^2$  and  $CHKSPZ$  was required to be less than 21 MeV/ $c^2$ .

After imposing the cuts in this subsection, 4553 events survived.

quantity	unit	resolution
kinetic energy $T_\mu$	MeV	$0.379 \times \sqrt{T_\mu}$
momentum $P_\mu$	MeV/c	$\sqrt{(0.0227P_\mu)^2 - (0.00784P_\mu)^4}$
azimuthal angle $\phi_\mu$	mrad	17.6
polar angle $\theta_\mu$	mrad	$32.2 \times \cos \theta_\mu$

TABLE I: Resolutions on the muon observables assumed in the kinematic fit to the  $K_{\mu 3\gamma}$  hypothesis.

### B. Kinematic fit

A least-squares fit was used to improve the resolution of the measured  $K_{\mu 3\gamma}$  quantities. We assumed just one undetected particle (neutrino) in the final state. The kinematic fit was applied to thirteen observables with three constraints. The observables were the kinetic energy of the charged particle, the momentum vector of the charged particle, and the momentum vectors of three photons. The directions of momentum vectors were defined to be from the kaon decay vertex position. The constraints were:

- The invariant mass of the total energy and momentum should be equal to the nominal mass of  $K^+$ ,
- The kinetic energy and momentum of the charged particle should be consistent with a muon hypothesis, and
- The invariant mass of one pair of photons should be equal to  $m_{\pi^0}$ .

There are three possible pairings of the three photons to form the  $\pi^0$ ; the combination which minimized the  $\chi^2$  of the global kinematic fit was chosen among the possible event topologies. In simulated  $K_{\mu 3\gamma}$  decays, 86% of the events that survived all the selection criteria were reconstructed with the correct pairing.

The kinematic fit was also applied with the assumption of  $K_{\mu 3}$  or  $K_{\pi 3}$  decay. To identify the  $K_{\mu 3}$  decay, the best combination of the two photons from the  $\pi^0$  was chosen as in the case of the fit to the  $K_{\mu 3\gamma}$  assumption, and the remaining photon was ignored. Figure 4(left) shows the invariant  $\gamma\gamma$  mass ( $M_{\gamma\gamma}$ ) distribution of the  $\pi^0$  from the  $K_{\mu 3}$  events. To identify the  $K_{\pi 3}$  decay, the events in which four photons were observed in the BL calorimeter were used but the photon with the lowest energy was ignored; the best combination of two photons to form the  $\pi^0$  was chosen so as to minimize the  $\chi^2$ . Figure 4(right) shows the  $M_{\gamma\gamma}$  distribution of the  $\pi^0$  from the  $K_{\pi 3}$  events. The results were used to select the events for calibrations and to check the performance of Monte Carlo simulation. The resolutions used for the muon and the photons in the fit on the  $K_{\mu 3\gamma}$  assumption, summarized in Table I and Table II, were obtained from the studies of the  $K_{\mu 3}$  events and the  $K_{\pi 3}$  events, respectively.

The  $\chi^2$  probability of the kinematic fit on the  $K_{\mu 3\gamma}$  assumption,  $Prob(\chi^2_{K_{\mu 3\gamma}})$ , was required to be more than

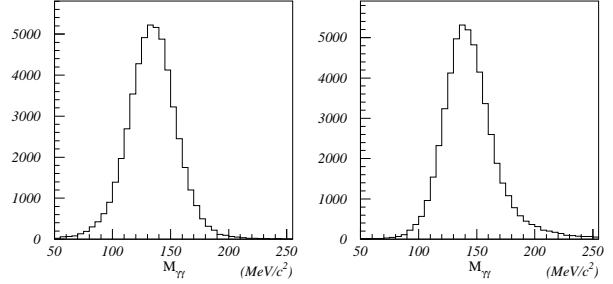


FIG. 4:  $M_{\gamma\gamma}$  distributions of the  $\pi^0$  from the  $K_{\mu 3}$ (left) and  $K_{\pi 3}$ (right) events.

quantity	unit	resolution
energy $E_\gamma$	MeV	$1.61 \times \sqrt{E_\gamma}$
azimuthal angle $\phi_\gamma$	mrad	39.8
polar angle $\theta_\gamma$	mrad	$65.6 \times \cos \theta_\gamma$

TABLE II: Resolutions on the photon observables assumed in the kinematic fit to the  $K_{\mu 3\gamma}$  hypothesis.

10%. In order to suppress the  $K_{\mu 3-1}$  background, the events whose  $\chi^2$  probability of the kinematic fit on the  $K_{\mu 3}$  assumption,  $Prob(\chi^2_{K_{\mu 3}})$ , was more than 10% were discarded. After imposing these  $\chi^2$  probability cuts, 360 events survived.

### C. Signal region

The following cuts were applied to the fitted observables of the surviving events. The energy of the undetected particle (neutrino) in the final state,  $E_\nu$ , should be larger than 60 MeV to suppress the  $K_{\pi 2\gamma}$  background. The invariant mass of the muon and neutrino was calculated and, in order to suppress the background events with  $\pi^+$  decay in flight, the invariant mass was required to be larger than 200 MeV/ $c^2$ . The polar angle of the neutrino momentum vector with respect to the beam axis should be larger than  $26^\circ$ , to prevent a photon in the final state from escaping along the beam direction. After imposing these cuts, 178 events survived.

Figure 5 shows the cosine of  $\theta_{\mu\gamma}$  versus  $E_\gamma$  plots of the events that survived all analysis cuts in real data and in Monte Carlo  $K_{\mu 3\gamma}$  simulation. The signal region was specified with  $E_\gamma > 30$  MeV and  $20^\circ < \theta_{\mu\gamma} < 60^\circ$  ( $0.50 < \cos(\theta_{\mu\gamma}) < 0.94$ ). The cut  $\theta_{\mu\gamma} < 60^\circ$  was required to improve the proportion of the correct pairing to  $\pi^0$  and to suppress the  $K_{\pi 3}$  background. Figure 6 and Figure 7 show the  $Prob(\chi^2_{K_{\mu 3\gamma}})$  distributions and the  $M_{\gamma\gamma}$  distribution of the  $\pi^0$ , respectively, from the events in the signal region in real data and in Monte Carlo  $K_{\mu 3\gamma}$  simulation. Forty events were observed in the signal re-

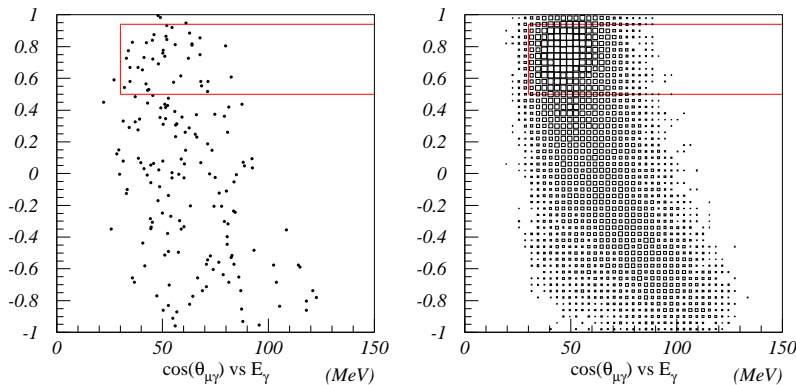


FIG. 5: Cosine of  $\theta_{\mu\gamma}$  versus  $E_\gamma$  plots of the events with all analysis cuts imposed in real data (left) and in the sample generated by Monte Carlo  $K_{\mu 3\gamma}$  simulation (right). The box indicates the signal region.

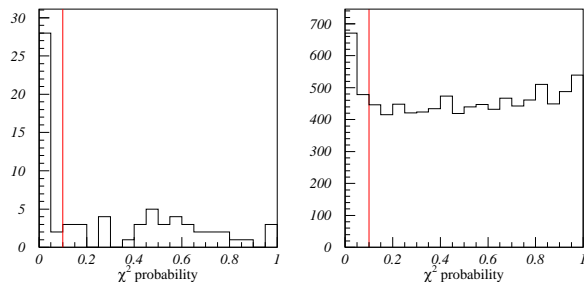


FIG. 6: Distributions of  $Prob(\chi^2_{K_{\mu 3\gamma}})$  from the events in the signal region in real data (left) and in the sample generated by Monte Carlo  $K_{\mu 3\gamma}$  simulation (right). All selection cuts except for the cut  $Prob(\chi^2_{K_{\mu 3\gamma}}) > 0.1$  in Subsection VIB are imposed.

gion.

## VII. BACKGROUND EXPECTATION

The  $K_{\mu 3-1}$  background was studied with real data from the  $3\gamma$  trigger. We used the timing of the photons relative to the muon track time,  $\Delta t_\gamma$ . The  $\Delta t_\gamma$  distributions of the two photons to form the  $\pi^0$  and of the radiative photon, after imposing all the offline cuts except for the timing cut to the photons ( $|\Delta t_\gamma| < 2$  nsec in Subsection VIA), are shown in Figure 8. Figure 9(left) shows the  $\cos(\theta_{\mu\gamma})$  versus  $E_\gamma$  plot of the events with a photon in the interval  $3 \text{ nsec} < |\Delta t_\gamma| < 6 \text{ nsec}$  in real data; the number of events in the signal region in Fig. 9(left) was 11. Assuming that the timing distribution of the BL cluster due to accidental hits was con-

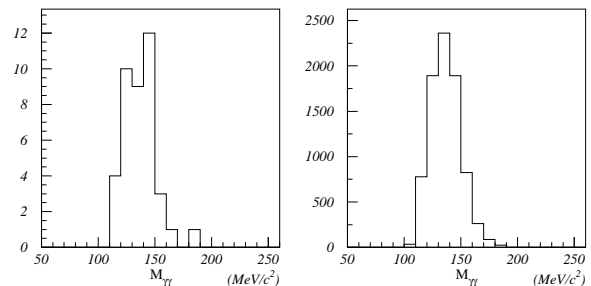


FIG. 7:  $M_{\gamma\gamma}$  distributions of the  $\pi^0$  from the events in the signal region in real data (left) and in the sample generated by Monte Carlo  $K_{\mu 3\gamma}$  simulation (right).

stant, the background level of  $K_{\mu 3-1}$  was estimated to be  $11/(6\text{nsec}/4\text{nsec}) = 7.3 \pm 2.2$  events.

Since it was difficult to isolate samples of the  $K_{\mu 3-2}$  and  $K_{\pi 2\gamma}$  backgrounds from the real data, these backgrounds were studied with the samples generated by Monte Carlo simulation. The background level of  $K_{\mu 3-2}$  was estimated to be  $< 0.35$  events at the 90% C.L. and was omitted from the background estimate. The background level of  $K_{\pi 2\gamma}$  was estimated to be  $0.38 \pm 0.08$  events.

The  $K_{e3(\gamma)}$  background was studied with the real data. The  $dE/dx$  cuts were inverted to enhance the  $e^+$  track events, but no event was left after imposing all the other analysis cuts. After taking into account the rejection efficiency of the inverted  $dE/dx$  cuts as well as the tagging efficiency of the inverted  $dE/dx$  cuts, the background level was estimated to be  $< 1.1$  events at the 90% C.L. The background level of  $K_{e3(\gamma)}$  was omitted from the background estimate.

The  $K_{\pi 3}$  background was studied with the real data,

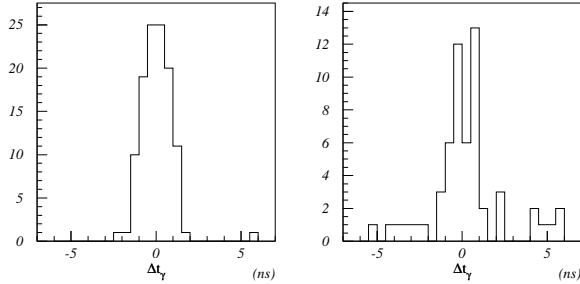


FIG. 8:  $\Delta t_\gamma$  distributions of the two photons to form the  $\pi^0$  (left) and of the radiative photon (right) in real data.

Source	Background level	Samples
$K_{\mu 3-1}$	$7.3 \pm 2.2$	Data
$K_{\mu 3-2}$	$< 0.35$ (90% C.L.)	MC
$K_{\pi 2\gamma}$	$0.38 \pm 0.08$	MC
$K_{e3(\gamma)}$	$< 1.1$ (90% C.L.)	Data
$K_{\pi 3}$	$8.8 \pm 1.6$	Data
Total	$16.5 \pm 2.7$	

TABLE III: Expected background levels in the signal region. “Data” and “MC” in the rightmost column indicate whether real data or Monte Carlo simulation were used for the estimation, respectively.

in particular with the muon identification cuts and the cuts to detect the extra photon. The studies of photon disappearance through the inefficiency of the BL, the inefficiency of the other subsystems, and the fused cluster in the BL were made with the BL cuts, the photon veto cuts, and the *DPSQ* and *CHKSPZ* cuts, respectively. Figure 9(right) shows the  $\cos(\theta_{\mu\gamma})$  versus  $E_\gamma$  plot of the events after imposing the inverted BL photon-veto cut (detection of the activity due to an extra photon in the BL calorimeter) in real data. The number of events in the signal region in Fig. 9(right) was 45 and, after taking into account the rejection of the offline BL photon-veto cut as well as the tagging efficiency of the inverted cut, the background level due to the inefficiency of the BL was estimated to be  $7.5 \pm 1.5$  events. With the similar method, the background levels due to the inefficiency of the other subsystems and due to the fused cluster in the BL were estimated to be  $0.8 \pm 0.6$  events and  $0.5 \pm 0.4$  events, respectively. The background level of  $K_{\pi 3}$  was  $8.8 \pm 1.6$  events in total.

The background levels are summarized in Table III. In total,  $16.5 \pm 2.7$  background events were expected in the signal region.

Acceptance factors		Samples
Muon trigger component (Section III)	0.140	MC
Photon trigger component (Section III)	0.00609	MC
Primary selection (Subsection IV B)	0.511	MC, $K_{\mu 2}$
Selection of muon and photons (Subsection VIA)	0.220	MC
Kinematic fit (Subsection VIB)	0.275	MC
Cuts after the kinematic fit (Subsection VIC)	0.649	MC
Signal region (Subsection VIC)	0.351	MC
Accidental loss (Section III and Subsection VIA)	0.669	$K_{\mu 2}, \pi_{scat}$
Total acceptance	$4.01 \times 10^{-6}$	

TABLE IV: Acceptance factors for the  $K_{\mu 3\gamma}$  decay in the kinematic region  $E_\gamma > 20$  MeV, and the samples used to determine them. “MC” in the rightmost column means the sample generated by Monte Carlo simulation. “ $K_{\mu 2}$ ” and “ $\pi_{scat}$ ” mean the data samples of  $K^+ \rightarrow \mu^+ \nu_\mu$  decays and scattered beam pions, respectively.

### VIII. SENSITIVITY

The acceptance factors for the selection criteria in this measurement (Table IV) were estimated primarily from Monte Carlo simulation. We generated the  $K_{\mu 3\gamma}$  sample at  $O(p^4)$  in ChPT with  $E_\gamma > 20$  MeV, which was set to be lower than the offline criteria on the photon energy<sup>2</sup>. In the simulated events, the kinetic energy and momentum of the muon and the energy and  $z$  position of the photons were smeared with deviates drawn from a Gaussian distribution to obtain measured resolutions on the observables (Table I and Table II). The acceptance of the primary selection to the Čerenkov counter, proportional chambers, beam counter and the target (Subsection IV B) and the acceptance loss by the accidental hits in the detector subsystems, in particular the loss due to the veto conditions in the trigger (Section III), were measured with data samples of  $K^+ \rightarrow \mu^+ \nu_\mu$  decays and scattered beam pions, which were simultaneously accumulated by the calibration triggers. The total acceptance was  $4.0 \times 10^{-6}$  and was dominated by the trigger acceptance.

The single event sensitivity (*SES*) for  $K_{\mu 3\gamma}$  was derived from the total acceptance, the total exposure of

<sup>2</sup> Thus, the acceptance factors and the single event sensitivity in this section are for the  $K_{\mu 3\gamma}$  decay in the kinematic region  $E_\gamma > 20$  MeV. In Section IX, we will first obtain the partial branching ratio for  $K_{\mu 3\gamma}$  in this kinematic region and then convert it into  $BR(K_{\mu 3\gamma}, E_\gamma > 30 \text{ MeV and } \theta_{\mu\gamma} > 20^\circ)$  and  $BR(K_{\mu 3\gamma}, 30 < E_\gamma < 60 \text{ MeV})$ .



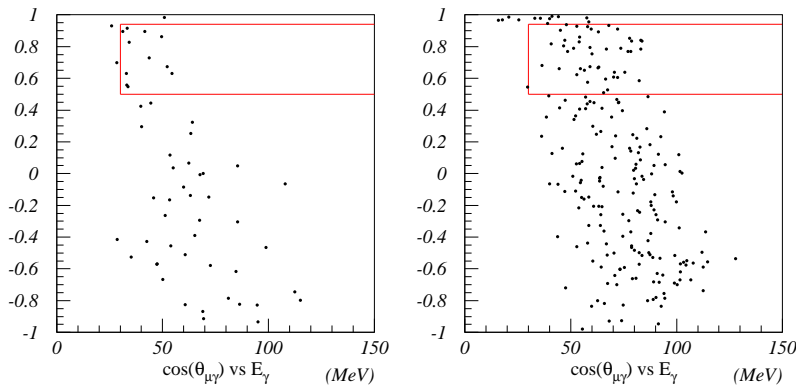


FIG. 9: Distributions in  $\cos(\theta_{\mu\gamma})$  versus  $E_\gamma$  of events selected as the  $K_{\mu 3-1}$ (left) and  $K_{\pi 3}$ (right) background events as described in the text. The box indicates the signal region.

Estimated systematic uncertainties	(%)
BL visible fraction	2.7
BL $z$ measurement	1.0
$e^+$ bremsstrahlung cut	1.0
Resolution in $T_\mu$ and $P_\mu$	2.8
Resolution in $E_\gamma$	1.5
Resolution in photon $z$ position	1.7
Monte Carlo statistical uncertainty	1.1
Total systematic uncertainty	4.9

TABLE V: Systematic uncertainties in the sensitivity and their estimates.

kaons entering the target ( $3.5 \times 10^{11}$  in Section III), and the fraction of kaons entering the target that decayed at rest (called the  $K^+$  stop efficiency,  $F_s$ ).  $F_s$  was measured to be  $0.669 \pm 0.014$  with the events of the IB component of the  $K_{\pi 2\gamma}$  decay, which were collected with the  $3\gamma$  trigger and selected<sup>3</sup> with the method used in the  $K_{\pi 2\gamma}$  analysis of E787 [14, 27]. Thus, the sensitivity for  $K_{\mu 3\gamma}$  was normalized to  $K_{\pi 2\gamma}$ <sup>4</sup> and many systematic uncertainties in the acceptance factors canceled.  $F_s$  was also measured

<sup>3</sup> The triggered events were further prescaled by eight, and were reconstructed with the assumption that the charged track was a  $\pi^+$ . After imposing primary cuts,  $\pi^+$  identification cuts, photon selection cuts and photon veto cuts, the kinematic fit with the assumption of the  $K_{\pi 2\gamma}$  decay was applied. The missing energy should be smaller than 141 MeV, and the  $\pi^+$  momentum  $P_{\pi^+}$  should satisfy  $140 < P_{\pi^+} < 180$  MeV/c. A total of 2425 events survived, with the background expectation of 3.6%. The contribution from the direct photon-emission component of the  $K_{\pi 2\gamma}$  decay was estimated to be 2.2%.

<sup>4</sup> The theoretical prediction for the IB component of the  $K_{\pi 2\gamma}$  branching ratio in the  $\pi^+$  kinetic energy region of 55 to 90 MeV,  $2.61 \times 10^{-4}$  [28], was used in this analysis. The Particle Data Group average,  $(2.75 \pm 0.15) \times 10^{-4}$  [8], confirmed this value.

with the  $K_{\pi 3}$  events collected with the  $3\gamma$  trigger, and the results were consistent. We obtained  $SES = 1.07 \times 10^{-6}$ . The systematic uncertainties in  $SES$  were due to:

- The BL calibration of the visible fraction and  $z$  measurement, to which the photon selection (Subsection VIA) was sensitive,
- The difference, between real data and Monte Carlo simulation, in the distributions of the variables to select the muon and three photons, in particular the variable on the  $e^+$  bremsstrahlung cut (Subsection VIA), and
- The smearing of the observables in the Monte Carlo events when the kinematic fit was applied.

The systematic uncertainties were studied from the observed sensitivity variation as each corresponding parameter was varied over the range that had not been excluded in the calibration. The statistical uncertainty of the Monte Carlo simulation in estimating the acceptance was also included. The systematic uncertainties are summarized in Table V. By adding them in quadrature, the total systematic uncertainty was estimated to be  $\pm 4.9\%$ .

## IX. RESULTS AND CONCLUSIONS

From the 40 observed events in the signal region, after subtracting the expected background ( $16.5 \pm 2.7$ ) we obtained  $23.5 \pm 6.9(stat.)$   $K_{\mu 3\gamma}$  events with the statistical uncertainty of 29%. With  $SES = (1.07 \pm 0.05(syst.)) \times 10^{-6}$ , the partial branching ratio for  $K_{\mu 3\gamma}$  in the kinematic region  $E_\gamma > 20$  MeV was  $(2.51 \pm 0.74(stat.) \pm 0.12(syst.)) \times 10^{-5}$ . The kinematic distributions of the observed 40 events were compared to the spectra predicted from the  $K_{\mu 3\gamma}$  decay plus all the background

contributions, as shown in Fig. 10. The  $\chi^2/\text{degree-of-freedom}$  values to evaluate the match between data and predictions were 2.7/6, 11.3/8, 12.5/5 and 7.0/9 in the distributions of  $E_\gamma$ ,  $\pi^0$  energy,  $E_\nu$  and muon momentum, respectively.

The factors 0.628 and 0.437, estimated from the theoretical  $K_{\mu 3\gamma}$  spectrum at  $O(p^4)$  in ChPT, are used to convert the measured partial branching fraction into  $BR(K_{\mu 3\gamma}, E_\gamma > 30 \text{ MeV and } \theta_{\mu\gamma} > 20^\circ)$  and  $BR(K_{\mu 3\gamma}, 30 < E_\gamma < 60 \text{ MeV})$ , respectively. Finally, the results of the measurement were:

$$BR(K_{\mu 3\gamma}, E_\gamma > 30 \text{ MeV and } \theta_{\mu\gamma} > 20^\circ) = (1.58 \pm 0.46(\text{stat.}) \pm 0.08(\text{syst.})) \times 10^{-5}$$

and

$$BR(K_{\mu 3\gamma}, 30 < E_\gamma < 60 \text{ MeV}) = (1.10 \pm 0.32(\text{stat.}) \pm 0.05(\text{syst.})) \times 10^{-5}.$$

The  $BR(K_{\mu 3\gamma}, E_\gamma > 30 \text{ MeV and } \theta_{\mu\gamma} > 20^\circ)$  was consistent with the theoretical prediction  $2.0 \times 10^{-5}$  [4, 5] as well as with the previous measurement  $(2.4 \pm 0.5(\text{stat.}) \pm 0.6(\text{syst.})) \times 10^{-5}$  in [9], and the  $BR(K_{\mu 3\gamma}, 30 < E_\gamma < 60$

MeV) was consistent with the previous measurement  $(1.5 \pm 0.4) \times 10^{-5}$  in [8]. The results of the E787 measurement provide better precision than the previous results.

### Acknowledgments

We acknowledge the contributions made by colleagues who participated in earlier phases of the E787 experiment, including M. Atiya, T.F. Kycia (deceased), D. Marlow, and A.J.S. Smith. We gratefully acknowledge the dedicated effort of the technical staff supporting this experiment and of the Brookhaven Collider-Accelerator Department. This research was supported in part by the U.S. Department of Energy under Contracts No. DE-AC02-98CH10886, No. W-7405-ENG-36, and Grant No. DE-FG02-91ER40671, by the Ministry of Education, Culture, Sports, Science and Technology of Japan through the Japan-US Cooperative Research Program in High Energy Physics and under the Grant-in-Aids for Scientific Research, for Encouragement of Young Scientists and for JSPS Fellows, and by the Natural Sciences and Engineering Research Council and the National Research Council of Canada.

- 
- [1] <http://www.phy.bnl.gov/e787/e787.html> .
- [2] J.F. Donoghue, E. Golowich, and B.R. Holstein, *Dynamics of the Standard Model* (Cambridge Univ. Press, Cambridge, 1992), and references therein.
- [3] B.R. Holstein, Phys. Rev. D **41**, 2829 (1990).
- [4] J. Bijnens, G. Ecker, and J. Gasser, in *DAΦNE Physics Handbook*, edited by L. Maiani, G. Pancheri, and N. Paver (Laboratori Nazionali di Frascati, Frascati, 1992).
- [5] J. Bijnens, G. Ecker, and J. Gasser, Nucl. Phys. B **396**, 81 (1993).
- [6] D. Ljung and D. Cline, Phys. Rev. D **8**, 1307 (1973).
- [7] O.G. Tchikilev *et al.*, arXiv:hep-ex/0506023, Phys. Atom. Nucl. **70**, 29 (2007).
- [8] Particle Data Group, C. Amsler *et al.*, Phys. Lett. B **667** 1 (2008).
- [9] S. Shimizu *et al.*, Phys. Lett. B **633** 190 (2006).
- [10] V.V. Braguta, A.A. Likhoded, and A.E. Chalov, Phys.Rev. D **65** 054038 (2002). The spectra of  $K_{\mu 3\gamma}$  observables are shown in the figure 3.
- [11] S. Adler *et al.*, Phys. Rev. Lett. **79**, 2204 (1997); S. Adler *et al.*, *ibid.* **84**, 3768 (2000).
- [12] S. Adler *et al.*, Phys. Lett. B **537**, 211 (2002); S. Adler *et al.*, Phys. Rev. D **70**, 037102 (2004).
- [13] S. Adler *et al.*, Phys. Rev. Lett. **88**, 041803 (2002).
- [14] S. Adler *et al.*, Phys. Rev. Lett. **85**, 4856 (2000).
- [15] S. Adler *et al.*, Phys. Rev. Lett. **85**, 2256 (2000); S. Adler *et al.*, Phys. Rev. D **63**, 032004 (2001); S. Adler *et al.*, *ibid.* **65**, 052009 (2002).
- [16] J. Doornbos *et al.*, Nucl. Instrum. Methods Phys. Res. A **444**, 546 (2000).
- [17] M.S. Atiya *et al.*, Nucl. Instr. Meth. Phys. Res. A **321**, 129 (1992).
- [18] E.W. Blackmore *et al.*, Nucl. Instr. Meth. Phys. Res. A **404**, 295 (1998).
- [19] M.S. Atiya *et al.*, Nucl. Instr. Meth. Phys. Res. A **279**, 180 (1989).
- [20] I-H. Chiang *et al.*, IEEE Trans. Nucl. Sci. **NS-42**, 394 (1995); T.K. Komatsubara *et al.*, Nucl. Instr. Meth. Phys. Res. A **404**, 315 (1998); D.A. Bryman *et al.*, *ibid.* **396**, 394 (1997).
- [21] W.R. Nelson *et al.*, SLAC Report No. SLAC 265 (1985).
- [22] S. Adler *et al.*, Phys. Rev. D **77**, 052003 (2008).
- [23] V.V. Anisimovskiy *et al.*, Phys. Rev. Lett. **93**, 031801 (2004).
- [24] A.V. Artamonov *et al.*, Phys. Lett. B **623**, 192 (2005).
- [25] A.V. Artamonov *et al.*, Phys. Rev. D **72**, 091102(R) (2005).
- [26] A.V. Artamonov *et al.*, Phys. Rev. Lett. **101**, 191802 (2008); A.V. Artamonov *et al.*, Phys. Rev. D **79**, 092004 (2009).
- [27] T. Tsunemi, Ph.D. Thesis, University of Tokyo, 2005.
- [28] G. D'Ambrosio, M. Miragliuolo, and P. Santorelli, in *DAΦNE Physics Handbook*, edited by L. Maiani, G. Pancheri, and N. Paver (Laboratori Nazionali di Frascati, Frascati, 1992).

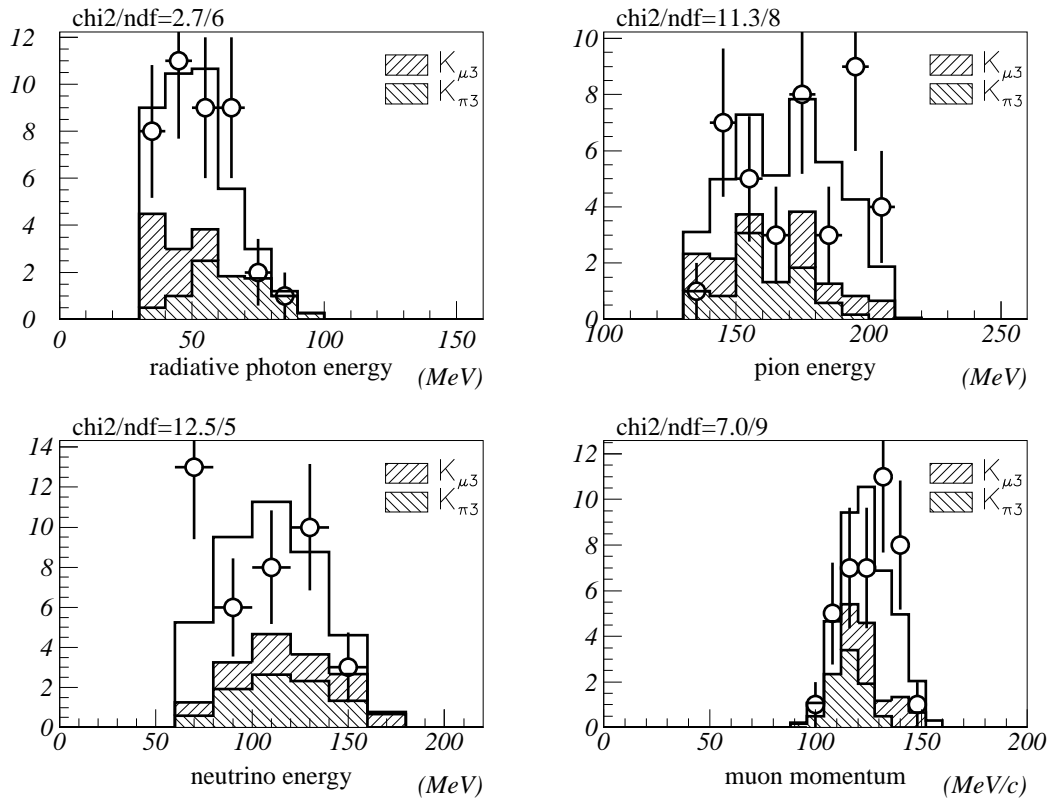


FIG. 10: Spectra of the  $K^+ \rightarrow \pi^0 \mu^+ \nu_\mu \gamma$  candidates:  $E_\gamma$  (top left),  $\pi^0$  energy (top right),  $E_\nu$  (bottom left) and muon momentum (bottom right). In each plot, the circles with error bars represent the distributions of the 40 events observed in the signal region. The conditions  $E_\gamma > 30$  MeV and  $E_\nu > 60$  MeV have been imposed in the analysis. The right-hatched and left-hatched histograms represent the expected distributions of the  $K_{\mu 3}$  and  $K_{\pi 3}$  backgrounds, respectively. The unhatched histogram represents the distribution of the Monte Carlo  $K_{\mu 3 \gamma}$  events with the central value of the measured branching ratio plus all the background contributions, and should be compared to the circles with error bars.